MESOSCALE POROELASTICITY OF HETEROGENEOUS MEDIA

Siavash Monfared[1]

Hadrien Laubie[2]

Farhang Radjai[3]

Roland Pellenq[4]

Franz-Josef Ulm[5]

ABSTRACT

Poromechanics of heterogeneous media is reformulated in a discrete framework using Lattice Element Method (LEM) that accounts for the presence of interfaces as well as local microtextural and elastic variations. The exchange of mechanical information between pore and solid(s) is captured by means of force field potentials for these domains, which eliminate the requirement of scale separability of continuum-based poromechanics approaches. In congruence with μVT and NPT ensembles of statistical mechanics, discrete expressions for Biot poroelastic coefficients are

[1]Department of Civil and Environmental Engineering, Massachusetts Institute of Technology, 77 Massachusetts Avenue, Cambridge, MA 02139, USA. Email: monfared@mit.edu.

[2]Department of Civil and Environmental Engineering, Massachusetts Institute of Technology, 77 Massachusetts Avenue, Cambridge, MA 02139, USA. Email: hlaubie@mit.edu.

[3]MultiScale Material Science for Energy and Environment UMI 3466 CNRS-MIT, MIT Energy Initiative, Massachusetts Institute of Technology, Cambridge, MA 02139, USA. Email: fradjai@mit.edu.

[4]MultiScale Material Science for Energy and Environment UMI 3466 CNRS-MIT, MIT Energy Initiative, Massachusetts Institute of Technology, Cambridge, MA 02139, USA. Email: pellenq@mit.edu.

[5]Department of Civil and Environmental Engineering, Massachusetts Institute of Technology, 77 Massachusetts Avenue, Cambridge, MA 02139, USA. Email: ulm@mit.edu.

derived. Considering harmonic-type interaction potentials for each link, analytical expressions for both isotropic and transversely isotropic effective elasticity are presented. The theory is validated against continuum based expressions of Biot poroelastic coefficients for porous media with isotropic and transversely isotropic elastic solid behavior.

INTRODUCTION

Poromechanics is dedicated to modeling and prediction of how porous materials deform in response to various external loadings. These loadings range from fluid-solid interactions by a variety of pressures at the liquid-solid interface to complex physical chemistry phenomena at the pore scale that produce a mechanical deformation (incl. fracture) of the solid. The classical backbone of poromechanics is based on continuum theories, ever since Maurice A. Biot defined the kinematics of deformation of the skeleton within the classical continuum mechanics framework as the reference for the description of flow of liquid phase through the pore space (Biot 1941), with the state equations for stress, $\boldsymbol{\Sigma}$, and porosity change, $\phi - \phi_0$, given in the linear poroelastic case by:

$$\boldsymbol{\Sigma} = \frac{1}{V}\frac{\partial E_{pot}}{\partial \mathbf{E}} = \mathbb{C} : \mathbf{E} - \mathbf{b}p \tag{1}$$

$$\phi - \phi_0 = -\frac{1}{V}\frac{\partial E_{pot}}{\partial p} = \mathbf{b} : \mathbf{E} + \frac{p}{\mathrm{N}} \tag{2}$$

where E_{pot} is the potential energy of the solid phase of the solid-pore composite of volume V, subjected to an average strain $\mathbf{E} = \langle \varepsilon \rangle_V$ at the boundary ∂V, and a pressure p at the solid-pore interface. $\mathbb{C}$ is the fourth-order elastic stiffness tensor, $\mathbf{b}$ is the second-order tensor of Biot pore pressure coefficients, and N denotes the solid Biot modulus. This continuum framework also provided the backbone for the development of the close-to-equilibrium thermodynamics framework of irreversible deformation of porous media pioneered by Coussy (Coussy 1995), and its extension to a large range of phase change and adsorption phenomena (Coussy 2010). In the same vein, microporomechanics theories can be viewed as refined extensions of the continuum framework to the microscale, in that they adapt continuum micromechanics theory (Suquet 1987; Zaoui 2002) to the specific nature of porous materials viewed as solid-pore composite materials (Dormieux

et al. 2002; Dormieux et al. 2006). While the continuum poromechanics theory has entered and transformed many engineering fields ranging from Civil- and Environmental Engineering and geophysics applications to biomechanics and the food industry (see for e.g. (Hellmich et al. 2013)), the intrinsic limitations of the theory relate to the very foundations of the continuum model, including scale separability and its impact on the relevance of the differential operators defining the momentum balance and displacement–strain operators. This is a serious limitation of the theory in its applicability to highly heterogeneous materials. For instance, such a continuum theory will fail for microstructure resolutions achieved by micro and nano Computed Tomography (CT) imaging techniques of highly heterogeneous materials, in which the characteristic length scale of the heterogeneity is of a similar scale as the sample size, or for multiscale heterogeneous materials for which a single representative elementary volume (rev) cannot be defined. It is for such systems that a discrete form of poromechanics theory is proposed, in which physical interactions replace volume descriptors. This approach is much akin to molecular representations of material systems with interaction forces between mass points derived from potentials that define the out-of-equilibrium state of the system w.r.t. a relaxed equilibrium configuration.

Herein, the elements of such a discrete poromechanics approach are developed using statistical mechanics ensemble definitions within the context of the Lattice Element Method (Topin et al. 2007; Affes et al. 2012) using the framework of effective potentials (Laubie et al. 2017b). By way of validation, some pore-solid morphologies are revisited to determine poroelastic constants within and beyond the classical continuum limits of scale separability.

LATTICE ELEMENT METHOD APPLIED TO PORE-SOLID COMPOSITES

Consider a porous material composed of a solid (volume V_s) and pore space (volume V_p). Following the Lattice Element Method (Topin et al. 2007; Affes et al. 2012; Laubie et al. 2017b), the two domains are discretized into a number of unit cells (or voxels), the center of which defines a mass point that interacts with a fixed number of neighboring mass points forming a regular or irregular lattice structure. The interaction forces and moments between two mass points i and j derive from an effective potential U_{ij} as a function of the translational, $\vec{\delta}_i = \vec{x}_i - \vec{X}_i$, and rotational,

$\vec{\vartheta}_i$, degrees of freedom, where $\vec{X}_i$ and $\vec{x}_i$ denote the position vectors of mass point i in the reference and the deformed configurations, respectively (for a detailed derivation, see (Laubie et al. 2017b)):

$$\vec{F}_i^j = -\frac{\partial U_{ij}}{\partial \vec{\delta}_i}; \quad \vec{F}_i^j + \vec{F}_j^i = \vec{0} \tag{3}$$

$$\vec{M}_i^j = -\frac{\partial U_{ij}}{\partial \vec{\vartheta}_i}; \quad \vec{M}_i^j + \vec{M}_j^i + \vec{r}_{ij} \times \vec{F}_j^i = \vec{0} \tag{4}$$

where $\vec{r}_{ij} = l_{ij}^0 \vec{e}_n^{ij}$ is the vector connecting node i to node j of rest-length l_{ij}^0 and oriented by the unit vector $\vec{e}_n^{ij}$ in a local orthonormal basis $(\vec{e}_n, \vec{e}_b, \vec{e}_t)$. For such discrete system, the stresses are modeled using the Virial expression (Christoffersen et al. 1981) $\boldsymbol{\sigma} = \rho_c \langle \vec{r} \otimes \vec{F} \rangle$, where ρ_c represents the number of interaction bonds per unit volume, $\langle . \rangle$ denotes the first moment of $\vec{r} \otimes \vec{F}$ distribution over interaction bonds; while neglecting the momentum term. In LEM for mass point i, this Virial expression can be written as:

$$\boldsymbol{\sigma}_i = \frac{1}{V_i} \sum_{j=1}^{N_i^b} \vec{r}_{ij} \otimes \vec{F}_i^j \tag{5}$$

with V_i denoting the volume of the unit cell, and N_i^b representing the number of node i's neighboring mass points. The Virial expression provides a truly discrete description of the system as opposed to the continuum-based stress definition employed in classical finite-element based approaches. The stress in volume V composed of a total of N_t unit cells is simply the volume average of the local stresses; that is:

$$\boldsymbol{\sigma} = \frac{1}{2V} \sum_{i=1}^{N_t} V_i \boldsymbol{\sigma}_i \tag{6}$$

What thus differs between different material domains is the interaction potential from which forces and moments are derived.

Effective Solid Potentials

The effective potential employed here for the solid phase(s) considers both two-body and three-body interactions between two mass points i and j, in the form:

$$U_{ij} = U_{ij}^s + U_{ij}^b \qquad \forall i \in V_s \tag{7}$$

where $U_{ij}^s = U_{ij}^s\left(\left(\vec{x}_j - \vec{x}_i\right)\cdot\vec{e}_n = \delta_j^n - \delta_i^n\right)$ stands for any suitable pairwise potential representative of the solid. For linear poroelastic systems this necessarily implies a harmonic expression for this pairwise potential:

$$U_{ij}^s = \frac{1}{2}\epsilon_{ij}^n\left(\frac{\delta_j^n - \delta_i^n}{l_{ij}^0}\right)^2 \tag{8}$$

with ϵ_{ij}^n denoting the axial energy parameter. Similarly, the three-body and rotational interactions read in the harmonic case (Laubie et al. 2017b):

$$\begin{aligned} U_{ij}^b \;=\; & \frac{1}{2}\epsilon_{ij}^t\left\{\left(\frac{\delta_j^b - \delta_i^b}{l_{ij}^0} - \vartheta_i^t\right)^2 + \left(\frac{\delta_j^t - \delta_i^t}{l_{ij}^0} + \vartheta_i^b\right)^2\right. \\ & + \left(\frac{\delta_j^b - \delta_i^b}{l_{ij}^0} - \vartheta_i^t\right)\left(\vartheta_i^t - \vartheta_j^t\right) + \left(\frac{\delta_j^t - \delta_i^t}{l_{ij}^0} + \vartheta_i^b\right)\left(\vartheta_j^b - \vartheta_i^b\right) \\ & \left. + \frac{1}{3}\left(\left(\vartheta_j^b - \vartheta_i^b\right)^2 + \left(\vartheta_i^t - \vartheta_j^t\right)^2\right)\right\} \end{aligned} \tag{9}$$

where ϵ_{ij}^t is the transverse energy parameter. With Eq. (7) at hand, the forces and moments read:

$$\left\{\begin{aligned} \vec{F}_i^j \;=\; -\frac{\partial U_{ij}}{\partial\vec{\delta}_i} \;=\; & \underbrace{\frac{\epsilon_{ij}^n}{l_{ij}^0}\left(\frac{\delta_j^n - \delta_i^n}{l_{ij}^0}\right)\vec{e}_n}_{F_i^{j,n}} + \underbrace{\frac{\epsilon_{ij}^t}{l_{ij}^0}\left(\frac{\delta_j^b - \delta_i^b}{l_{ij}^0} - \frac{1}{2}\left(\vartheta_j^t + \vartheta_i^t\right)\right)\vec{e}_b}_{F_i^{j,b}} + \underbrace{\frac{\epsilon_{ij}^t}{l_{ij}^0}\left(\frac{\delta_j^t - \delta_i^t}{l_{ij}^0} + \frac{1}{2}\left(\vartheta_j^b + \vartheta_i^b\right)\right)\vec{e}_t}_{F_i^{j,t}} \\ \vec{M}_i^j \;=\; -\frac{\partial U_{ij}}{\partial\vec{\vartheta}_i} \;=\; & \underbrace{-\frac{\epsilon_{ij}^t}{2}\left(\frac{\delta_j^t - \delta_i^t}{l_{ij}^0} + \frac{1}{3}\left(\vartheta_j^b + 2\vartheta_i^b\right)\right)\vec{e}_b}_{M_i^{j,b}} + \underbrace{\frac{\epsilon_{ij}^t}{2}\left(\frac{\delta_j^b - \delta_i^b}{l_{ij}^0} - \frac{1}{3}\left(\vartheta_j^t + 2\vartheta_i^t\right)\right)\vec{e}_t}_{M_i^{j,t}} \end{aligned}\right. . \tag{10}$$

It should be noted that the defined harmonic potentials are merely Taylor expansions of non-harmonic potentials around the equilibrium state of the system in LEM (Laubie et al. 2017b). Thus, the linear poroelastic formulation herein presented could be extended to non-linear poroelastic systems when considering non-harmonic potentials without much loss of generality. Additionally, one can calibrate the energy parameters to reproduce an effective elastic behavior based on the lattice and the network chosen. This point will be developed further in the Application section for

two different elastic symmetries.

Effective Pore-Pressure Force Field Potential

The simplest case to consider the deformation behavior of the solid phase due to a pressure in the pore space is the saturated drained situation, in which the fluid in the pore domain is assumed to communicate with an outside reservoir maintained at a constant pressure p, so that in the relaxed state, the same pressure will prevail in the pore domain. Such a hydrostatic drained stress state, $\boldsymbol{\sigma} = -p\mathbf{1}$, necessarily implies that only central-forces are active on each mass point in the pore domain, $\vec{F}_i^j = F_i^{j,n}\vec{e}_n$ so that the Virial stress expression for the entire pore domain of volume V_p and N_p voxels becomes:

$$\boldsymbol{\sigma} = -p\mathbf{1} = \frac{n_\ell^p}{2V_p}\langle r_{ij}F_i^{j,n}\vec{e}_n \otimes \vec{e}_n\rangle = \frac{1}{2V_p}\sum_{i=1}^{N_p}\sum_{j=1}^{N_i^b} r_{ij}\, F_i^{j,n}\, \vec{e}_n^{ij} \otimes \vec{e}_n^{ij} \tag{11}$$

where n_ℓ^p denotes number of links in the pore domain. In a zeroth-order description of the microtexture, $F_i^{j,n}$ and r_{ij} are considered to be independently distributed and thus not correlated (Radjai et al. 1998; Radjai et al. 2009; Azema and Radjai 2014) which allows Eq. (11) to be expressed as $\boldsymbol{\sigma} = \frac{n_\ell^p}{2V_p}\langle rF^n\rangle\langle\vec{e}_n \otimes \vec{e}_n\rangle$, which leads to the equality of traces:

$$3p = \frac{n_\ell^p}{2V_p}\langle rF^n\rangle \tag{12}$$

Now, by way of analogy with logarithmic equations of state for bulk fluids (Poirier and Tarantola 1998), consider a logarithmic potential, $U\left(r_{ij}\right) = \omega \ln\left(l_{ij}^0/r_{ij}\right)$, and hence $F_i^{j,n} = -\partial U/\partial r_{ij} = \omega/r_{ij}$, where $\omega = \langle rF^n\rangle$ (of dimension of work) can be viewed as a fluid characteristic and should be constant. $\langle rF^n\rangle$ can be made independent of r_{ij} (which is dependent on the orientation $\vec{e}_n$ of the bonds) by simply setting:

$$F_i^{j,n} = -\frac{6p}{r_{ij}}\frac{V_p}{n_\ell^p} \tag{13}$$

This relation ensures that the mean pressure is p and the equality (12) is satisfied. This paves the way for imposing a pressure inside a domain discretized by a regular lattice:

$$p = -\frac{\omega n_\ell^p}{6V_p} \tag{14}$$

Equation (13) defines the interaction between pore and solid mass points in the form of externally supplied work. This perturbation of the system's equilibrium is resolved through the theory of minimum potential energy as a new equilibrium position is sought through energy minimization (see (Laubie et al. 2017b)). Lastly, it is readily recognized that $\langle \vec{e}_n \otimes \vec{e}_n \rangle$ is the fabric tensor, $\mathbf{H}^p$, characterizing the morphology of the pore space. It can be expanded in the following way:

$$\mathbf{H}^p = \frac{1}{n_\ell^p} \sum_{i=1}^{N_p} \sum_{j=1}^{N_i^b} \vec{e}_n \otimes \vec{e}_n \tag{15}$$

For Eq. (11) to hold, the fabric tensor, Eq. (15), should be diagonal, $\mathbf{H}^p = \frac{1}{3}\,\mathrm{tr}\,(\mathbf{H}^p)\,\mathbf{1}$ with no deviatoric components, i.e. $\mathrm{dev}\,(\mathbf{H}^p) = \mathbf{H}^p - 1/3\,\mathrm{tr}\,(\mathbf{H}^p)\,\mathbf{1} = \mathbf{0}$, which holds true for any regular lattice. Furthermore, $\mathrm{tr}\,(\mathbf{H}^p)$=1 by construction. Note that, if the underlying lattice is not regular and hence not diagonal, then the values of $F_i^{j,n}$ would have been dependent not only on the average pressure to be imposed, but also the orientations of the bonds.

POROELASTIC PROPERTIES AND ENSEMBLE DEFINITIONS

The poroelastic properties of materials form much of the backbone of application of the poromechanics theory. This includes the elasticity tensor, $\mathbb{C}$, the tensor of Biot coefficients, $\mathbf{b}$, and the solid Biot modulus N. From the composite structure of porous materials, it is readily understood that these macroscopic properties call for averages. Such averages are best defined, in statistical mechanics, within the context of specific statistical ensembles which –at least theoretically– include every possible microscopic state of the system. The advantage of using statistical ensembles for the determination of the poroelastic properties is that each ensemble is associated with a characteristic state function or thermodynamic potential that uniquely define –upon minimization– the equilib-

rium state of the system in function of a few observable parameters; much akin to the classical minima theorems of elasticity employed in continuum mechanics, e.g. for the derivation of the state equations of poroelasticity (1) and (2) (Dormieux et al. 2002; Dormieux et al. 2006). It is thus shown that making the link between statistical ensembles and such boundary conditions is quite helpful for the determination of the poroelastic constants from discrete simulations.

Drained Elasticity Properties in the NVT-Ensemble

The first quantity of interest is the drained elasticity tensor, which is obtained by letting $p \sim \omega = 0$. In this drained situation, a regular displacement boundary condition is prescribed at the boundary (∂V) of the simulation box:

$$\vec{\xi} = \mathbf{E} \cdot \vec{x} \qquad \forall \vec{x} \in \partial V \tag{16}$$

where $\mathbf{E}$ refers to macroscopic strain tensor. Such a mechanical boundary condition is akin to an NVT-ensemble (or canonical ensemble) at the *composite* (solid + pore) scale, in that the total number of particles N_t is constant, the volume (or more generally, the displacement) of the system (V) is controlled via the boundary condition (16), and temperature (T) is maintained constant. The thermodynamic potential that defines such an ensemble is the Helmholtz free energy Ψ of the composite system, which realizes a minimum value at equilibrium ($r \rightarrow r_0$). Given the mechanical boundary value problem ($\mathbf{E}$,$p = 0$), the minimum of the Helmholtz free energy is strictly equivalent to the minimum of the potential energy of the solid phase subjected at its boundary to the (displacement) boundary condition, Eq. (16), and a zero pressure in the pore space; and coincides with the free energy of the solid phase(s):

$$E^s_{pot}(\mathbf{E}) = \Psi\left(N_t, V, T\right) = \min_{\vec{\delta}_i, \vec{\vartheta}_i} \sum_{links\ ij \in V^s_0} U_{ij}\left(\vec{\delta}_j - \vec{\delta}_i + \vec{r}_{ij} \times \vec{\vartheta}_i;\ \vec{\vartheta}_j - \vec{\vartheta}_i\right) \tag{17}$$

The fourth-order stiffness tensor is then obtained by considering the curvature of the potential energy of the system around the relaxed state ($r \rightarrow r_0$):

$$\mathbb{C} = \frac{1}{V} \frac{\partial}{\partial \mathbf{E}} \left(\frac{\partial E^s_{pot}}{\partial \mathbf{E}} \right) \Bigg|_{\omega=0; r \rightarrow r_0} \tag{18}$$

Biot Pore Pressure Coefficients in the μVT-Ensemble

The determination of the tensor of the Biot pore pressure coefficients, **b**, and the solid's Biot modulus, N, requires some further considerations. From the first macroscopic state equation, Eq. (1), it is realized that the tensor of Biot coefficients is obtained from the average stresses in an experiment where the strain, **E**, is zero, while a constant pressure p prevails in the pore space; exerting this pressure onto the solid–pore interface. Such conditions are akin to the Grand canonical ensemble or μVT ensemble at the *composite* (solid + pore) scale, in that (1) the porous system is open at a specified chemical potential μ; and (2) the overall volume is conserved with $\mathbf{E} = \mathbf{0}$; and (3) the temperature, T, is maintained constant. In this μVT-ensemble, the characteristic state function that needs to be minimized is the so called Landau potential (or Grand potential), $\Omega(\mu, V, T) = \Psi - \mu N_f$, where Ψ is the Helmholtz free energy, μ the chemical potential and N_f the number of particles (here fluid particles). For the open system, the free energy is the sum of the free energy of the solid (Ψ_s) and of the fluid phase (Ψ_f) [see (Coussy 1995) for a detailed derivation of the thermodynamics of the porous continuum as an open system]; and the latter is but the difference between the potential energy of the fluid at constant pressure (μN_f) and the work by the fluid in the pore space; i.e. $\Psi_f = \mu N_f - p\left(V^p - V^p_0\right)$ (where V^p and V^p_0 stand for the pore volumes respectively after and before deformation; i.e. $V^p = V\phi$; $V^p_0 = V\phi_0$, with ϕ the Lagrangian porosity). The Landau potential for the composite system thus reduces to the classical expression of the potential energy of the solid phase for the considered boundary conditions ($\mathbf{E} = \mathbf{0}, p$); that is:

$$E^s_{pot}(\mathbf{E} = \mathbf{0}, p) \equiv \Omega(\mu, V, T) = \min_{\vec{\delta}_i, \vec{\vartheta}_i} \left(\Psi^{(\mu VT)}_s - pV(\phi - \phi_0) \right) \tag{19}$$

where $\Psi_s^{(\mu VT)} = \sum_{links\ ij \in V_0^s} U_{ij}\left(\vec{\delta}_j - \vec{\delta}_i + \vec{r}_{ij} \times \vec{\vartheta}_i;\ \vec{\vartheta}_j - \vec{\vartheta}_i\right)$ is the Helmholtz free energy of the solid phase.

With the characteristic state function thus defined, the inter-particle forces $\vec{F}_i^j$ in the solid domain are readily determined, permitting the determination of the stress via the virial expression in the composite μVT ensemble:

$$\boldsymbol{\Sigma}^{(\mu VT)} = \frac{1}{2V}\sum_{i\in V}\sum_{j=1}^{N_i^b} \vec{r}_{ij} \otimes \vec{F}_i^j = -\left(\frac{1}{2V}\sum_{i\in V_s}\sum_{j=1}^{N_i^b} \vec{r}_{ij} \otimes \vec{F}_i^j + \phi_0 p\mathbf{1}\right) \tag{20}$$

where the first term on the r.h.s. of Eq. (20) is the contribution of the solid phase with inter-particle forces $\vec{F}_i^j = \partial\Psi_s^{(\mu VT)}/\partial\vec{r}_{ij}$, whereas the second term represents the contribution of the pressure prevailing in the (Lagrangian) porosity, $\phi_0 = \left(V_p/V\right)$, with pressure p defined by Eq. (14). A straightforward comparison with the classical equation of state of poroelasticity, Eq. (1), thus leads to the following definition of the second-order tensor of Biot pore pressure coefficients, $\mathbf{b}$:

$$\mathbf{b} = -\frac{\boldsymbol{\Sigma}^{(\mu VT)}}{p} = \frac{1}{p}\left(\frac{1}{2V}\sum_{i\in V_s}\sum_{j=1}^{N_i^b} \vec{r}_{ij} \otimes \vec{F}_i^j\right) + \phi_0\mathbf{1} \tag{21}$$

Hence, all what it takes to obtain the tensor of Biot coefficient is to determine, in the μVT ensemble, the inter-particle forces $\vec{F}_i^j$ in the solid domain that result from the pore-pressure loading using the Landau potential expression (19).

Biot Modulus in the NPT-Ensemble

The classical way of determining the Biot modulus is by means of the so-called unjacketed test, originally proposed by Biot and Willis (Biot and Willis 1957). The test consists of placing a sample into a pressure vessel maintained at the same pressure p as the fluid in the pore space. Such test conditions are akin to the isothermal–isobaric, NPT–ensemble of the *solid* phase (i.e. at the constituent scale, in contrast to the composite scale), in that (1) the number of solid particles N_s are maintained constant, (2) the solid is subjected at its (entire) boundary ∂V_s to a pressure p, while (3) the temperature, T, is maintained constant. The thermodynamic potential that characterizes the

NPT-ensemble is the Gibbs free energy of the solid phase, $G(N_s, p, T)$, which strictly coincides for the pressure boundary condition to which the solid is subjected to the solid's potential energy:

$$E^s_{pot} \equiv G(N_s, p, T) = \min_{\vec{\delta}_i, \vec{\vartheta}_i} \left(\Psi^{(NPT)}_s - W_p \right) \tag{22}$$

where $\Psi^{(NPT)}_s$ is the Helmholtz free energy of the solid phase in the considered ensemble:

$$\Psi^{(NPT)}_s = \sum_{links\ ij \in V^s_0} U_{ij} \left(\vec{\delta}_j - \vec{\delta}_i + \vec{r}_{ij} \times \vec{\vartheta}_i;\ \vec{\vartheta}_j - \vec{\vartheta}_i \right) \tag{23}$$

while $W_p = -p \left(V^s - V^s_0 \right)$ is the external work realized by the prescribed pressure p on the solids boundary, with $V^s - V^s_0 = V_0 (E_v - (\phi - \phi_0))$ the volume change of the solid phase; that is:

$$W_p = -pV_0 (E_v - (\phi - \phi_0)) \tag{24}$$

Herein, $E_v = (V - V_0)/V_0 = \mathbf{1} : \mathbf{E}$ is the relative volume variation of the simulation box and $\phi - \phi_0$ represents the change of the (Lagrangian) porosity, compared to the reference porosity ϕ_0. Evaluation of (22) thus requires measurements of the volume strain (E_v) and the porosity change ($\phi - \phi_0$) in the simulations (as classically done in laboratory tests using the unjacketed test). Around the equilibrium state, defined by harmonic interactions, such determination can be circumvented, when evoking Clapeyron's formula which permits a direct determination of the free energy of the solid, in the NPT ensemble, from the external work; i.e., $W_p = 2\Psi^{(NPT)}_s$. This in turn provides a direct means to assess the porosity change from both Eq. (2) and (24):

$$(\phi - \phi_0) = \mathbf{b} : \mathbf{E} + \frac{p}{\mathrm{N}} = \mathbf{1} : \mathbf{E} + \frac{2\Psi^{(NPT)}_s}{pV_0} \tag{25}$$

Finally, it should be noted that under the considered boundary conditions in the isothermal-isobaric ensemble (relative to the solid), the effective stress obtained from the Virial expression is zero:

$$\boldsymbol{\Sigma}^{(NPT)} + p\mathbf{1} = \frac{1}{2V}\sum_{i\in V_s}\sum_{j=1}^{N_i^b}\vec{r}_{ij}\otimes\vec{F}_i^j + (1-\phi_0)\,p\mathbf{1} = \mathbf{0} \tag{26}$$

where the interaction forces, $\vec{F}_i^j$, are obtained by minimizing the potential energy in this isothermal-isobaric ensemble (i.e., Eq. (22)). Expanding Eq. (25 with strain tensor $\mathbf{E} = -\mathbb{S} : (\mathbf{1}-\mathbf{b})\,p$ and $\mathbb{S} = \mathbb{C}^{-1}$, the drained compliance tensor of the composite as predicted by Eq. (1) for $\boldsymbol{\Sigma}^{(NPT)}+p\mathbf{1} = \mathbf{0}$, leads to the solid Biot modulus:

$$\frac{1}{\mathrm{N}} = \frac{2\Psi_s^{(NPT)}}{p^2V_0} - (\mathbf{1}-\mathbf{b}) : \mathbb{S} : (\mathbf{1}-\mathbf{b}) \tag{27}$$

It should be emphasized that this determination of the Biot modulus is strictly valid only when the behavior of the solid phase is defined by harmonic potentials, for which Clapeyron's formula applies. This still holds for non-harmonic potentials around the equilibrium state, $r \longrightarrow r_0$, for which most non-harmonic potential expressions (e.g. Lennard-Jones) degenerate to harmonic expressions. The Biot modulus is thus confirmed as a measure of the solid's elasticity around the equilibrium state, much akin to the drained elasticity tensor, as defined by Eq. (18).

APPLICATION

By way of application, the proposed discrete model of poroelasticity is implemented for Simple Cubic (SC) lattice systems. The LEM-approach here employed follows the approach developed by Laubie et al. (Laubie et al. 2017b) for solids, where specific details about calibration and numerical implementation of the method can be found. In short, for all the cases considered herein, a cubic simulation box of side length $L = a_0\,(n-1)$ composed of $(n-1)^3$ unit cells of size a_0 are employed, where n stands for the number of mass points in any given direction. The mass points form a regular lattice with their interactions encapsulated by a network of links that connects a mass point to its 26 neighboring mass points. Thus, mechanical information are propagated through this

lattice network in 13 directions. This forms the so-called D3Q26 lattice structure consisting of 6 box-links of rest-length $l^0 = a_0$, 8 cross-diagonal links of length $\sqrt{3}a_0$, and 12 in-plane-diagonal links of length $\sqrt{2}a_0$ (see Fig. 1).

Solid Potential Parameter Calibration

With a focus on linear poroelasticity, the interactions between mass points of the solid phase(s) (volume V_s) are defined by harmonic potentials, requiring the calibration of the energy parameters $\epsilon_{ij}^{(n,t)}$ for mass points i belonging to a specific solid phase and link $j = 1, 26$, with the understanding that links in same directions have same energy parameters. These energy parameters define the curvature of the potential energy around the equilibrium state, in the sense of expressions (17) and (18) for a pure solid phase subjected at its boundary to the regular displacement condition (16). It is thus readily understood that the $2 \times 13 = 26$ energy parameters, $\epsilon_{ij}^{(n,t)}$, need to be calibrated with respect to the elasticity of the solid, expressed by stiffness tensor $\mathbb{C}^s$. However, the choice of lattice/network used imposes some constraints on the range of elastic behavior that can be captured. This is consistent with the current understanding of the link between texture (here lattice structure) and deformation behavior of materials (Greaves et al. 2011). Specifically, in the isotropic case, it has been shown that the D3Q26 lattice structure in LEM, with non-negative normal and tangential energy parameters $\epsilon_{ij}^{(n,t)} \geq 0$, is able to capture the following range of solid Poisson's ratios (Laubie et al. 2017b):

$$-1 \leq \nu^s = \frac{C_{13}^s}{\left(C_{11}^s + C_{13}^s\right)} \leq 1/4 \tag{28}$$

where the Voigt notations for stiffness constants is employed; i.e. $C_{11}^s = C_{1111}^s$, $C_{13}^s = C_{1133}^s$. The upper bound in (28) is the limit on Poisson's ratios for the central-force lattice, when three-body interactions are neglected ($\epsilon_{ij}^t = 0$). For $\nu > 1/4$, one needs to consider a different combination of lattice/network (see e.g. (Norris 2014)). Given isotropic symmetry, a maximum of 6 non-zero energy parameters can be used to calibrate the isotropic elastic behavior. For $0 \leq \nu^s \leq 1/4$, among possible calibrations, only three non-zero energy parameters are required $\left(\epsilon_1^n, \epsilon_1^t\right)$ for the 6 box-links of rest-length $l^0 = a_0$, and ϵ_4^n for the 12 in-plane-diagonal links of length $\sqrt{2}a_0$ (for

numbering of the links, see Fig. 1). Considering a discretization by n mass points of unit cell size a_0, the following explicit parameterization of these energy parameters in function of the isotropic plane-strain modulus, $M^s = C^s_{11} - \left(C^s_{13}\right)^2 / C^s_{11} = E^s / \left(1 - (\nu^s)^2\right)$ (with E^s = Young's modulus) and the Poisson's ratio $\nu^s \in [0, 1/4]$ is obtained:

$$\begin{cases} \dfrac{\epsilon^n_1}{M^s a_0^3} = \dfrac{(n-1)^2}{n^2} \dfrac{(1-3\nu^s)(1-\nu^s)}{1-2\nu^s} \\ \dfrac{\epsilon^n_4}{M^s a_0^3} = \dfrac{(n-1)}{n} \dfrac{\nu^s(1-\nu^s)}{1-2\nu^s} \\ \dfrac{\epsilon^t_1}{M^s a_0^3} = \dfrac{(n-1)^2}{n^2} \dfrac{(1-4\nu^s)(1-\nu^s)}{1-2\nu^s} \end{cases} \tag{29}$$

From this parametrization it is also recognized that the three energy parameters are not independent, but related by the Poisson's ratio:

$$\frac{\epsilon^t_1}{\epsilon^n_1} = \frac{(1-4\nu^s)}{(1-3\nu^s)} \leq 1; \quad \frac{\epsilon^n_4}{\epsilon^n_1} = \frac{n}{n+1} \frac{\nu^s}{(1-3\nu^s)} \tag{30}$$

That is, one energy parameter is required in the isotropic case, with the other ones being scaled by Poisson's ratio of the solid.

Similar restrictions can be derived for transversely isotropic materials, for which the non-zero components of the stiffness tensor – in Voigt notation – are $C^s_{11} = C^s_{22}$, C^s_{12}, $C^s_{13} = C^s_{23}$, C^s_{33}, $C^s_{44} = C^s_{55}$, while $C^s_{11} - C^s_{12} = 2C^s_{66}$; namely (Laubie et al. 2017b):

$$C^s_{12} \leq C^s_{66} \left(\text{i.e., } C^s_{12} \leq \frac{1}{3} C^s_{11}\right); \; C^s_{13} \leq C^s_{44} \tag{31}$$

Considering rotational material symmetry around the $\vec{e}_3-$axis, there are, a priori, a total of 8 energy parameters that can be used for fitting the elastic properties, which reduce (thanks to the condition $C_{11} - C_{12} = 2C_{66}$) to six; namely $\left(\epsilon^n_1, \epsilon^t_1\right)$ and $\left(\epsilon^n_4, \epsilon^t_4\right)$ for links in the plane of symmetry $\vec{e}_1 \times \vec{e}_2$ [$\left(\epsilon^n_1, \epsilon^t_1\right)$ for the 4 box-links of rest length $l^0 = a_0$ oriented in the $\vec{e}_1-$ and $\vec{e}_2-$ directions, and $\left(\epsilon^n_4, \epsilon^t_4\right)$ for the 4 in-plane diagonals of length $\sqrt{2}a_0$; see Fig. 1] and ϵ^n_3 and ϵ^n_6 for links in the $\vec{e}_3 \times \vec{e}_1$

and $\vec{e}_3 \times \vec{e}_2$ plane [ϵ_3^n for the 2 box-links oriented in the $\vec{e}_3-$direction; and ϵ_6^n for the 8 in-plane diagonals of length $\sqrt{2}a_0$; Fig. 1], for which the non-zero elastic constants of the transversely isotropic material are linearly linked to the energy parameters by:

$$\begin{pmatrix} C_{11}^s \\ C_{12}^s \\ C_{33}^s \\ C_{13}^s \\ C_{44}^s \\ C_{11}^s - C_{12}^s - 2C_{66}^s = 0 \end{pmatrix} = \frac{1}{a_0^3} \begin{bmatrix} \frac{n^2}{(n-1)^2} & \frac{n}{2(n-1)} & 0 & \frac{n}{2(n-1)} & 0 & \frac{n}{n-1} \\ 0 & \frac{n}{2(n-1)} & 0 & 0 & 0 & -\frac{n}{2(n-1)} \\ 0 & 0 & \frac{n^2}{(n-1)^2} & \frac{n}{n-1} & 0 & \frac{n}{n-1} \\ 0 & 0 & 0 & \frac{n}{2(n-1)} & 0 & -\frac{n}{2(n-1)} \\ 0 & 0 & 0 & \frac{n}{2(n-1)} & \frac{n^2}{2(n-1)^2} & \frac{n}{2(n-1)} \\ \frac{n^2}{(n-1)^2} & -\frac{n}{n-1} & 0 & \frac{n}{2(n-1)} & -\frac{n^2}{(n-1)^2} & \frac{n}{n-1} \end{bmatrix} \begin{pmatrix} \epsilon_1^n \\ \epsilon_4^n \\ \epsilon_3^n \\ \epsilon_6^n \\ \epsilon_1^t \\ \epsilon_4^t \end{pmatrix} \tag{32}$$

Continuum Micromechanics Reference Solutions

A cubic simulation box of size $L = a_0\,(n-1)$, with a centric spherical pore of different pore radius R corresponding to different porosities is considered:

$$\phi_0 = \frac{n_p}{(n-1)^3} \tag{33}$$

where $(n-1)^3$ is the total number of mass points discretizing the solid and the pore volumes, and n_p the number of mass points defining the pore space in a simple cubic lattice. The focus of the validation examples is to compare the poroelastic properties one obtains using the discrete approach with analytical expressions of microporomechanics based on the assumption of scale separability. In this vein, the pore morphology herein considered is akin to a matrix-pore inclusion microtexture often associated with the Mori-Tanaka effective estimates (Mori and Tanaka 1973; Beneviste 1987) for which linear homogenization methods provide the following expressions for (1) the drained stiffness tensor (Dormieux et al. 2002; Dormieux et al. 2006):

$$\mathbb{C} = (1-\phi_0)\,\mathbb{C}^s : \langle \mathbb{A} \rangle_{V_s} \tag{34}$$

(2) the tensor of Biot pore pressure coefficients, with $\phi_0\mathbf{1}$ and $\mathbf{1}$ as its lower and upper bounds, respectively:

$$\mathbf{b} = \mathbf{1} : (\mathbb{I} - \mathbb{S}^s : \mathbb{C}) \tag{35}$$

and (3) the solid Biot modulus:

$$\frac{1}{\mathrm{N}} = \mathbf{1} : \mathbb{S}^s : (\mathbf{b} - \phi_0\mathbf{1}) \tag{36}$$

where $\langle\mathbb{A}\rangle_{V_s}$ in Eq. (34) is the average strain localization tensor over the solid phase (V_s). In continuum micromechanics, the strain localization tensor links the macroscopic strain $\mathbf{E}$ imposed as a boundary condition (16) to the continuous microstrains $\varepsilon\left(\vec{z}\right) = \mathbb{A}\left(\vec{z}\right) : \mathbf{E}$ into the solid phase, $\forall\vec{z} \in V_s$. In general, the average strain localization tensor for the rth phase given a matrix stiffness $\mathbb{C}^s$, reads:

$$\langle\mathbb{A}\rangle_r = [\mathbb{I} + \mathbb{P} : (\mathbb{C}^r - \mathbb{C}^s)]^{-1} : \langle[\mathbb{I} + \mathbb{P} : (\mathbb{C}^r - \mathbb{C}^s)^{-1}]\rangle_V^{-1} \tag{37}$$

with $\mathbb{P}$, the generalized Hill concentration tensor defined as (Zaoui 2002):

$$P_{ijkl} = -\left(\frac{\partial^2}{\partial x_j \partial x_l}\int_\Omega G_{ik}\left(\vec{x} - \vec{x}'\right)\right)_{(ij)(kl)} \tag{38}$$

where (ij)(kl) indicates symmetrization, and $G_{ij}(\vec{x} - \vec{x}')$ is the second order Green's tensor for generalized linear elastic anisotropic media. In the micro- and macro- isotropic case, i.e. $\mathbb{C} = 3K\mathbb{J} + 2G\mathbb{K}$ and $\mathbf{b} = \mathrm{b}\mathbf{1}$, the previous relations simplify, for a matrix-inclusion microtexture, as follows (Dormieux et al. 2006):

$$\frac{K}{k^s} = \frac{4g^s\left(1-\phi_0\right)}{3k^s\phi_0 + 4g^s} \tag{39}$$

$$\frac{G}{g^s} = \frac{\left(9k^s + 8g^s\right)\left(1-\phi_0\right)}{\left(6\phi_0 + 9\right)k^s + \left(12\phi_0 + 8\right)g^s} \tag{40}$$

$$\mathrm{b} = 1 - \frac{K}{k^s} \tag{41}$$

$$\frac{1}{\mathrm{N}} = \frac{\mathrm{b} - \phi_0}{k^s} \tag{42}$$

For the transversely isotropic case, the effective elasticity can be obtained from Eq. (34) while expressions (35) and (36) in this case, i.e. $\mathbf{b} = \mathrm{b}_1\left(\mathbf{1} - \vec{e}_3 \otimes \vec{e}_3\right) + \mathrm{b}_3 \vec{e}_3 \otimes \vec{e}_3$, read:

$$\mathrm{b}_1 (= \mathrm{b}_2) = 1 - \left(S^s_{11} + S^s_{12}\right)(C_{11} + C_{12}) - S^s_{13}(C_{11} + C_{12} + 2C_{13}) - S^s_{33} C_{13} \tag{43}$$

$$\mathrm{b}_3 = 1 - 2S^s_{11} C_{13} - 2S^s_{12} C_{13} - 2S^s_{13}(C_{13} + C_{33}) - S^s_{33} C_{33} \tag{44}$$

$$\frac{1}{\mathrm{N}} = 2(\mathrm{b}_1 - \phi_0)\left(S^s_{11} + S^s_{12} + S^s_{13}\right) + (\mathrm{b}_3 - \phi_0)\left(2S^s_{13} + S^s_{33}\right) \tag{45}$$

For comparison of the elasticity content in the transversely isotropic case, the indentation moduli expressions for transversely isotropic materials are employed, which nicely condense the different macro- and micro-stiffness parameters into two single elasticity parameters that can be probed in contact experiments, in and normal to the axis of rotational symmetry (Delafargue and Ulm 2004):

$$\frac{M_3(x_3)}{m^s_3} = \frac{2}{m^s_3}\sqrt{\frac{C_{11}C_{33} - C^2_{13}}{C_{11}}\left(\frac{1}{C_{44}} + \frac{2}{\sqrt{C_{11}C_{33}} + C_{13}}\right)^{-1}} \tag{46a}$$

$$\frac{M_1(x_1)}{m^s_1} \simeq \frac{1}{m^s_1}\sqrt{\sqrt{\frac{C_{11}}{C_{33}}}\frac{C^2_{11} - C^2_{12}}{C_{11}} M_3} \tag{46b}$$

where m^s_3 and m^s_1 are the indentation moduli of the solid phase. These continuum micromechanics solutions are strictly valid only in the case of scale separability between the size of the heterogeneity (pore size $R/a_0 = \left(\frac{3}{4\pi} n_p\right)^{1/3}$) and the size of the representative volume element (r.e.v. size $L/a_0 = (n-1)$); and hence for $n_p \ll \frac{4\pi}{3}(n-1)^3$, a condition to be challenged in the LEM simulations. The continuum relations are thus an ideal target to compare with the discrete solutions, using Eq. (18) for the elasticity, and the ensemble definitions of the tensor of Biot coefficients (21) and of the solid Biot modulus (27), respectively.

Validation Results

Cubic simulation boxes of different lengths L={50,70,90}, with $a_0 = 1$, were considered with a spherical pore centered inside. The pore radius, R, was gradually increased, with a maximum pore radius - to - box size ratio $R/L = 0.45$ corresponding to a porosity $\phi_0 = \frac{4\pi}{3}(R/L)^3 = 0.38$. The

case of isotropic solid behavior, defined by a bulk modulus $k^s = 20$ GPa and a Poisson's ratio of $\nu^s = 0.2$ is considered first. The energy parameters $\epsilon_{ij}^{(n,t)}$ for the solid were thus calibrated using Eq. (29). The effective stiffness tensor $\mathbb{C}$ was obtained through evaluation of Eq. (18) by considering, in the simulations, appropriate displacement boundary conditions as defined in Eq. (16). Figure 2a compares the simulation results with the effective stiffness coefficients obtained from the Mori-Tanaka homogenization scheme, Eqs. (39) and (40). Furthermore, the effective moduli, K and $G(= C_{44})$, are displayed in Figs. 2c and 2e, respectively. Next, poroelastic properties are considered by first focusing on the μVT ensemble and the discrete definition of Biot pore pressure coefficient, b. A pressure $p/k^s = 0.05$ is imposed inside the pore space using Eq. (14) in the μVT ensemble. Utilizing the theorem of minimum potential energy as stated in Eq.(22), inter-particle forces $\vec{F}_i^j$ induced from the pore-pressure loading are obtained. This paves the way to evaluate b from Eq. (21). Figure 3a compares the simulation results with the reference solution (41), using either the previously determined effective bulk moduli, K (labeled "Direct" in Fig. 2c) or the Mori-Tanaka estimate (labeled "MT" in Fig. 2c) via Eq. (39). Lastly, Biot solid modulus, N, is obtained by considering its NPT ensemble definition (25), which in the isotropic case reads:

$$\frac{1}{\mathrm{N}^{(NPT)}} = \frac{2U^{(NPT)}}{p^2 V_0} - \frac{3\,(\mathrm{b}-1)^2}{C_{11}+2C_{12}} \tag{47}$$

The evaluation is achieved here by prescribing, in the simulations, a pressure $p/k^s = 0.05$ both inside the pore space utilizing Eq. (14) and on the boundaries of the simulation box. Thus, all it takes for obtaining N from Eq. (47) is the computation of the free energy of the solid, $U^{(NPT)}$, once the structure finds its new equilibrium through Eq. (22), and the previously determined Biot coefficient. Figure 3b displays the comparison between the NPT-simulation results, using b from discrete theory in the μVT ensemble labeled as "LEM $(NPT)^*$" and b determined directly from simulated effective elasticity in LEM, labeled as "LEM $(NPT)^{**}$" against its continuum reference solution, Eq. (42), labeled in Figure 3b as "Direct". The same cubic simulation boxes were considered for validating the transversely isotropic poroelastic properties obtained from simulation vis-á-vis their continuum

counterparts. To this end, the energy parameters $\epsilon_{ij}^{(n,t)}$ were calibrated using Eq. (32) to reproduce the following solid elastic properties, $C_{11}^s = 55$ GPa, $C_{12}^s = 10$ GPa, $C_{13}^s = 14$ GPa, $C_{33}^s = 28$ GPa, and $C_{44}^s = 17$ GPa, and thus the solid indentation moduli (according to Eq.46), $m_3^s = 31.8$ GPa, and $m_1^s = 48.7$ GPa. Figure 2b shows the comparison of the simulated effective elasticity against the continuum values from the matrix-pore inclusion model captured via Mori-Tanaka effective estimates. Furthermore, the elasticity content is condensed into the normalized indentation moduli (46) and compared with the continuum matrix-pore inclusion (Mori-Tanaka) model, Eq. (34), as displayed in Figures 2d and 2f. Using the same μVT simulation strategy as in the isotropic case, a pore pressure loading normalized by the average Voigt-Reuss-Hill (VRH) bulk modulus for materials with hexagonal symmetry (see e.g. (Berryman 2005)), $p/k_{VRH}^s = 0.05$ is imposed. Figures (4a) and (4b) display a comparison of the μVT simulation results of the Biot coefficients of the considered transversely isotropic medium, $\mathbf{b} = \mathrm{b}_1 \left(\mathbf{1} - \vec{e}_3 \otimes \vec{e}_3\right) + \mathrm{b}_3 \vec{e}_3 \otimes \vec{e}_3$, with the analytical solutions (43) and (44) using as inputs either the simulated effective elasticity obtained by LEM, labeled as "Direct" or the analytical homogenized elasticity as obtained from Eq. (34), labeled "MT". Finally, a comparison of the NPT simulation results with the analytical expression (45) is shown in Figure 4c, displaying the evolution of the solid Biot modulus N with R/L. In the evaluation of N from the NPT simulation results (i.e. same pressure $p/k_{VRH}^s = 0.05$ imposed on the pore wall and on the simulation box), a specification of Eq. (25) for the transversely isotropic case reads:

$$\frac{1}{\mathrm{N}^{(NPT)}} = \frac{2U^{(NPT)}}{p^2 V_0} - \left(\frac{2C_{11}\left(\mathrm{b}_1 - 1\right)^2}{\left(C_{11} - C_{12}\right)\left(C_{11} + 2C_{12}\right)} + \frac{\left(\mathrm{b}_3 - 1\right)\left(\left(\mathrm{b}_3 - 1\right)\left(C_{11} + C_{12}\right) - 4C_{13}\left(\mathrm{b}_1 - 1\right)\right)}{C_{33}\left(C_{11} + C_{12}\right) - 2C_{13}^2} \right) \tag{48}$$

where $U^{(NPT)}$ is the free energy of the solid links in the NPT ensemble, while the effective elasticity C_{ij} and Biot coefficients b_1 and b_3 are previously determined by simulations (see Figs. 2b, 4a and 4b).

DISCUSSIONS

The idealized structures considered in this study represent a microtexture best captured by

the Mori-Tanaka homogenization scheme. The Mori-Tanaka scheme is often associated with a matrix-inclusion microtexture where the matrix phase overshadows the mechanical response of the inclusion phase(s), while considering interactions between inclusions (in contrast to the dilute scheme; see, for instance, (Dormieux et al. 2006)). Furthermore, for a two-phase composite with spherical inclusions, the Mori-Tanaka scheme corresponds to the Hashin-Shtrikman bounds (Weng 1984) and specifically for spherical voids, the upper Hashin-Shtrikman bound. However, it is worth noting that the presented methodology to estimate poroelastic properties of heterogeneous media is independent of microtextures being considered.

While the discrete simulation results compare well against their continuum poroelastic counterparts for both the isotropic and the transversely isotropic cases, a deviation is observed at higher porosity values that merit further discussion. Specifically, for small porosities, $\phi_0 < 5\times10^{-3}$ (or $R/L \leq 0.1$), the two approaches provide similar results. This is not surprising since – within this limit – scale separability, delineating the domain of application of the continuum models (here the Mori-Tanaka model) strictly applies. Beyond that limit, however, the results obtained from the discrete and the continuum approach begin to differ. One possible reason for the observed deviations is related to finite size effects associated with the finite size of the simulation box, noting that the elementary voxel size (a_0) remains much smaller than the size of the elementary heterogeneity at high porosities. To explore this further, two quantities, $\delta_{iso.}$ and $\delta_{ti.}$ are defined to capture any deviations from the imposed elastic solid symmetry for the isotropic and transversely isotropic cases; that is, for the isotropic case:

$$\delta_{iso.} = \frac{|C_{44} - \frac{1}{2}(C_{11} - C_{12})|}{C_{44}} \times 100 \tag{49}$$

and for the transversely isotropic case:

$$\delta_{ti.} = \frac{|C_{66} - \frac{1}{2}(C_{11} - C_{12})|}{C_{66}} \times 100 \tag{50}$$

Using the elasticity constants C_{ij} obtained from the simulations, Figs. 2g and 2h plot $\delta_{iso.}$ and $\delta_{ti.}$ vs. R/L, showing that for $R/L > 0.1$ the effective (i.e. composite) elasticity content captured by the

simulations departs from the material symmetries of the solid phase. Within the range of considered values, $\delta_{iso.} \leq 4$ in the isotropic case and $\delta_{ti.} \leq 8$ in the transversely isotropic case. On the other hand, the simulation results deviate from the continuum solution for the poroelastic constants (see Figs. 2a, 2b), for which the continuum solutions (i.e. Eqs. (41), (42) in the isotropic case, and Eqs. (43) through (45) for the transversely isotropic case) hold irrespective of elastic homogenization scheme. Thus, the observed deviation between discrete simulations and continuum calculations in the high porosity limit for elastic and poroelastic properties seem to be rooted in the finite size of the system as it challenges both the application of Eshelby's solution for an ellipsoidal inclusion in an infinite medium (Eshelby 1957) and Mori-Tanaka homogenization scheme's subjection of inclusions to the first moment (mean) of matrix stresses (Mori and Tanaka 1973; Beneviste 1987). The same deviation is observed for highly disordered systems (Laubie et al. 2017a) but attributed to the high stress concentrations between pore walls. In this vein, the probability density function (pdf) of normalized solid stresses of the considered idealized pore-matrix structures in the μVT ensemble are plotted in Fig. 5 for three different R/L ratios. In violation of scale separability, for $R/L = 0.157$ and $R/L = 0.229$ normalized stresses follow Gaussian distributions. However, the long tails for $R/L = 0.443$ indicate areas of high stress concentration, a feature not captured by mean-field based theories of micromechanics. This is intimately related to the requirement of scale separability in homogenization theory. A key property of scale separability exploited in the theory of homogenization is that the local problem cannot see the boundaries (Pavliotis and Stuart 2007) which clearly is violated in cases of high R/L ratios studied here.

Surface energy effects are incorporated in poromechanics by making a distinction between the free energy stored elastically into the solid matrix, ψ_s, and energy u stored at the solid-fluid interface; such that $\Psi_s = \psi_s(\mathbf{E}, p) + u(\mathbf{E}, p)$, with the energy balance for the interface at equilibrium expressed as (Vandamme et al. 2010; Brochard et al. 2012):

$$du = \tilde{\sigma}^s ds \tag{51}$$

where $\tilde{\sigma}^s$ denotes surface stress and s represents the actual area of the pore walls per unit volume of porous material in its reference configuration. Furthermore, for example in the case of adsorption in a linearly elastic isotropic porous material, one can obtain material parameters α_ϵ and α_φ, to quantify strain and porosity changes due to surface stresses, respectively (Vandamme et al. 2010). In this vein, the proposed method can be extended to capture adsorption-induced structural phase transitions in a porous material employing an osmotic ensemble (Snurr et al. 1993; Mehta and Kofke 1994; Coudert et al. 2011):

$$\Omega_{os.}(T,P) = \Psi_s + PV - \int_0^P N_{ads.}(T,p)\, V_m(T,p)\, dp \tag{52}$$

where T, P, Ψ_s, V, $N_{ads.}$ and V_m are temperature, pressure, the free energy of the solid in the absence of adsorbed molecules, the volume of the porous host, the number of adsorbed molecules inside the host, and the molar volume of the adsorbing species in its bulk state, respectively. Then, one seeks for the structure that minimizes $\Omega_{os.}$. Once this structure is obtained, $N_{ads.}(T,P)$ can be predicted with standard Grand Canonical Monte Carlo (GCMC) simulations. Classically, the main challenge of using Eq. (52) is access to Ψ_s, which would be readily available via LEM.

CONCLUSIONS

As the resolution of microtexture and heterogeneity of porous materials is progressing rapidly thanks to advancements in e.g. CT-imaging techniques (Hubler et al. 2017), there is a need to adapt the tools of poromechanics to model and to predict the deformation of porous materials in response to various external loadings. The discrete poromechanics approach proposed and implemented in the Lattice Element Method (LEM) aims at contributing to this effort, well beyond the classical mean-field based theories of continuum microporomechanics which do not capture microtextural information beyond one-point correlation functions and confined in its application by the scale separability condition. Specifically, the discrete nature of the approach provides access to local stresses and displacements as well as force flow in a heterogeneous system, which can illuminate the path for understanding stress and strain localization in a multiphase porous composite, and form

a basis for subsequent refinements to include irreversible deformation (incl. fracture), deformation during flow, and so on. The following points of observation deserve attention:

1. The discrete approach herein proposed considers a porous materials as an ensemble of mass points that interact via forces and moments that derive from effective potentials. Illustrated here for harmonic potentials for both 2-body and 3-body interactions, it is thus readily understood that both the solid and the composite responses are relevant for linear poroelastic theory only. However, this linear discrete poromechanics model can, in a straightforward manner, be extended to the nonlinear case through the consideration of non-harmonic effective potentials (such as Lennard-Jones, Morse potential, and so on), whose Taylor expansion around the (undeformed) equilibrium configuration is the harmonic case. Otherwise said, the calibration procedure herein suggested for the interaction energies ('well-depth') remain valid and just need to be refined to calibrate the nonlinear potential parameters. As such, LEM can be contrasted with finite-element based approaches, as it provides a consistent framework to coarse grain interaction potentials validated at a lower scale.
2. Re-formulated within the context of statistical physics, the discrete approach thus derived provides access to the classical poroelastic properties of highly heterogeneous porous materials as macroscopic properties relevant to specific statistical ensemble definitions. It was thus shown, that the results from an μVT-ensemble provide access to the tensor of Biot pore pressure coefficients, $\mathbf{b}$, while the results from an NPT-ensemble permit determination of the Biot solid modulus, N. To achieve this goal, an original reformulation of drained pressure conditions was proposed to translate pressure in the pore space into interaction forces. While the approach was here derived for a constant pressure prevailing in the pore space, it could equally be applied to varying pressures prevailing in the pore space. The approach as such could thus possibly be used for coupled flow-deformation problems, and via some minor adaptation for partially saturated situations, which will be reported in future work.

3. The discrete approach herein proposed removes by its very nature the assumption of scale separability that delineates continuum microporomechanics approaches. This opens new insights into the intimate interplay between constituent behavior and composite behavior of porous materials. The proposed approach can be viewed as a powerful tool to link micro- to macro-behavior of porous materials; specifically for porous materials exhibiting a large size range of heterogeneities that does not permit scale separation.

ACKNOWLEDGMENT

This work was funded by X-Shale Hub: the Science and Engineering of Gas Shale, a collaboration between Shell, Schlumberger, and the Massachusetts Institute of Technology, enabled through MIT's Energy Initiative. The Authors would like to acknowledge Vincent Richefeu (Universite Joseph Fourier), Jean-Yves Delenne (Montpellier SupAgro) and Saeid Nezamabadi (Universite de Montpellier) who provided the backbone of the LEM code used for simulations. FR would like to acknowledge the support of the ICoME2 Labex (ANR-11-LABX-0053) and the A*MIDEX projects (ANR-11-IDEX-0001-02) cofunded by the French program Investissements d'Avenir, managed by the French National Reseach Agency (ANR). The authors would also like to thank the reviewers for their insightful comments.

REFERENCES

Affes, R., Delenne, J.-Y., Monerie, R., Radjai, F., and Topin, V. (2012). "Tensile strength and fracture of cemented granular aggregates." *Eur. Phys. J.E.*, 35(117).

Azema, E. and Radjai, F. (2014). "Internal structure of inertial granular flows." *Phys. Rev. Lett.*, 112(7).

Beneviste, Y. (1987). "A new approach to the application of mori-tanaka's theory in composite materials." *Mech. Mater.*, 6(2).

Berryman, J. (2005). "Bounds and self-consistent estimates for elastic constants of random polycrystals with hexagonal, trigonal, and tetragonal symmetries." *J. Mech. Phys. Solids*, 53(10).

Biot, M. (1941). "General theory of three-dimensional consolidation." *J. Appl. Phys.*, 12(2).

Biot, M. and Willis, D. (1957). "The elastic coefficients of the theory of consolidation." *J. Appl. Mech.*, 24.

Brochard, L., Vandamme, M., and Pellenq, R.-M. (2012). "Poromechanics of microporous media." *J. Mech. Phys. Solids*, 60.

Christoffersen, J., Mehrabadi, M., and Nemat-Nasser, S. (1981). "A micromechanical description of granular material behavior." *J. Appl. Mech.*, 48(2).

Coudert, F.-X., Boutin, A., Jeffroy, M., Mellot-Draznieks, C., and Fuchs, A. (2011). "Thermodynamic methods and models to study flexible metal-organic frameworks." *ChemPhysChem*, 12.

Coussy, O. (1995). *Mechanics of porous continua*. Wiley and Sons, Chichester, England.

Coussy, O. (2010). *Mechanics and physics of porous solids*. Wiley and Sons, Chichester, England.

Delafargue, A. and Ulm, F.-J. (2004). "Explicit approximations of the indentation modulus of elastically orthotropic solids for conical indenters." *Int. J. Solids. Struct.*, 41(26).

Dormieux, L., Kondo, D., and Ulm, F.-J. (2006). *Microporomechanics*. Wiley and Sons, Chichester.

Dormieux, L., Molinary, A., and Kondo, D. (2002). "Micromechanical approach to the behavior of poroelastic materials." *J. Mech. Phys. Solids*, 50(10).

Eshelby, J. (1957). "The determination of the elastic field of an ellipsoidal inclusion, and related

problems." *Proc. R. Soc. A.*, 241.

Greaves, G., Greer, A., Lakes, R., and Rouxel, T. (2011). "Poisson's ratio and modern materials." *Nat. Mater.*, 10.

Hellmich, C., Pichler, B., and Adam, D. (2013). "Poromechanics v: Proceedings of the fifth biot conference on poromechanics." Amer Society of Civil Engineers.

Hubler, M., Gelb, J., and Ulm, F.-J. (2017). "Microtexture analysis of gas shale by xrm imaging." *J. Nanomech. Micromech.*, 7(3).

Laubie, H., Monfared, S., Radjai, F., Pellenq, R.-M., and Ulm, F.-J. (2017a). "Disorder-induced stiffness degradation of highly disordered porous materials." *J. Mech. Phys. Solids* . In press.

Laubie, H., Monfared, S., Radjai, F., Pellenq, R.-M., and Ulm, F.-J. (2017b). "Effective potential and elastic properties in the lattice-element method: Isotropy and transverse isotropy." *J. Nanomech. Micromech.*, 7(3).

Mehta, M. and Kofke, D. (1994). "Coexistence diagrams of mixtures by molecular simulation." *Chem. Eng. Sci.*, 49.

Mori, T. and Tanaka, K. (1973). "Average stress in matrix and average elastic energy of materials with misfitting inclusions." *Acta Metallurgica*, 21(5).

Norris, A. (2014). "Mechanics of elastic networks." *Proc. R. Soc. A.*, 470.

Pavliotis, G. and Stuart, A. (2007). *Multiscale Methods - Averaging and Homogeniation*. Springer.

Poirier, J. and Tarantola, A. (1998). "A logaritmic equation of state." *Phys. Earth. Planet. Int.*, 109(1-2).

Radjai, F., Delenne, J.-Y., Azema, E., and Roux, S. (2009). "Force and fabric states in granular media." *Granular Matter*, 35(1145).

Radjai, F., Wolf, D., Jean, M., and Moreau, J.-J. (1998). "Bimodal character of stress transmission in granular packings." *Phys. Rev. Lett.*, 80(1).

Snurr, R., Bell, A., and Theodorou, D. (1993). "Prediction of adsorption of aromatic hydrocarbons in silicalite from grand canonical Monte Carlo simulations with biased insertions." *J. Phys. Chem.*, 97(51).

585 Suquet, P. (1987). *Elements of homogenization for inelastic solid mechanics*.

586 Topin, V., Delenne, J.-Y., Radjai, F., Brendel, L., and Mabille, F. (2007). "Strength and failure of
587 cemented granular matter." *Eur. Phys. J.E.*, 23(413).

588 Vandamme, M., Brochard, L., Lecampion, B., and Coussy, O. (2010). "Adsorption and strain: The
589 CO2-induced swelling of coal." *J. Mech. Phys. Solids*, 58(10).

590 Weng, G. J. (1984). "Some elastic properties of reinforced solids with special reference to isotropic
591 ones containing spherical inclusions." *Int. J. Eng. Sci.*, 22, 845–856.

592 Zaoui, A. (2002). "Continuum micromechanics: A survey." *J. Eng. Mech.*, 128(8).

List of Figures

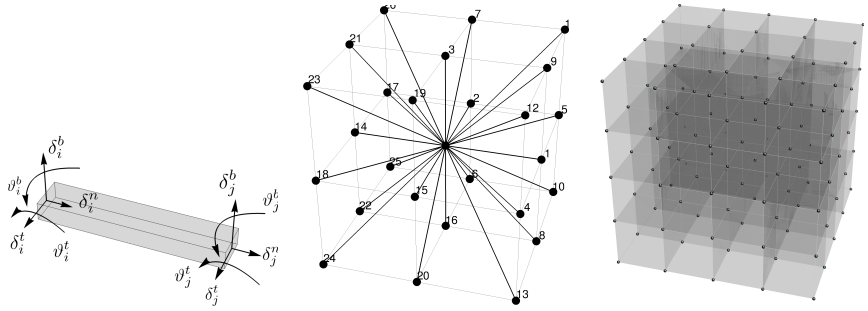
δ_i^b
ϑ_i^b
δ_i^n
δ_i^t
ϑ_i^t
δ_j^b
ϑ_j^b
δ_j^n
ϑ_j^t
δ_j^t
(a)
(b)
(c)

Fig. 1

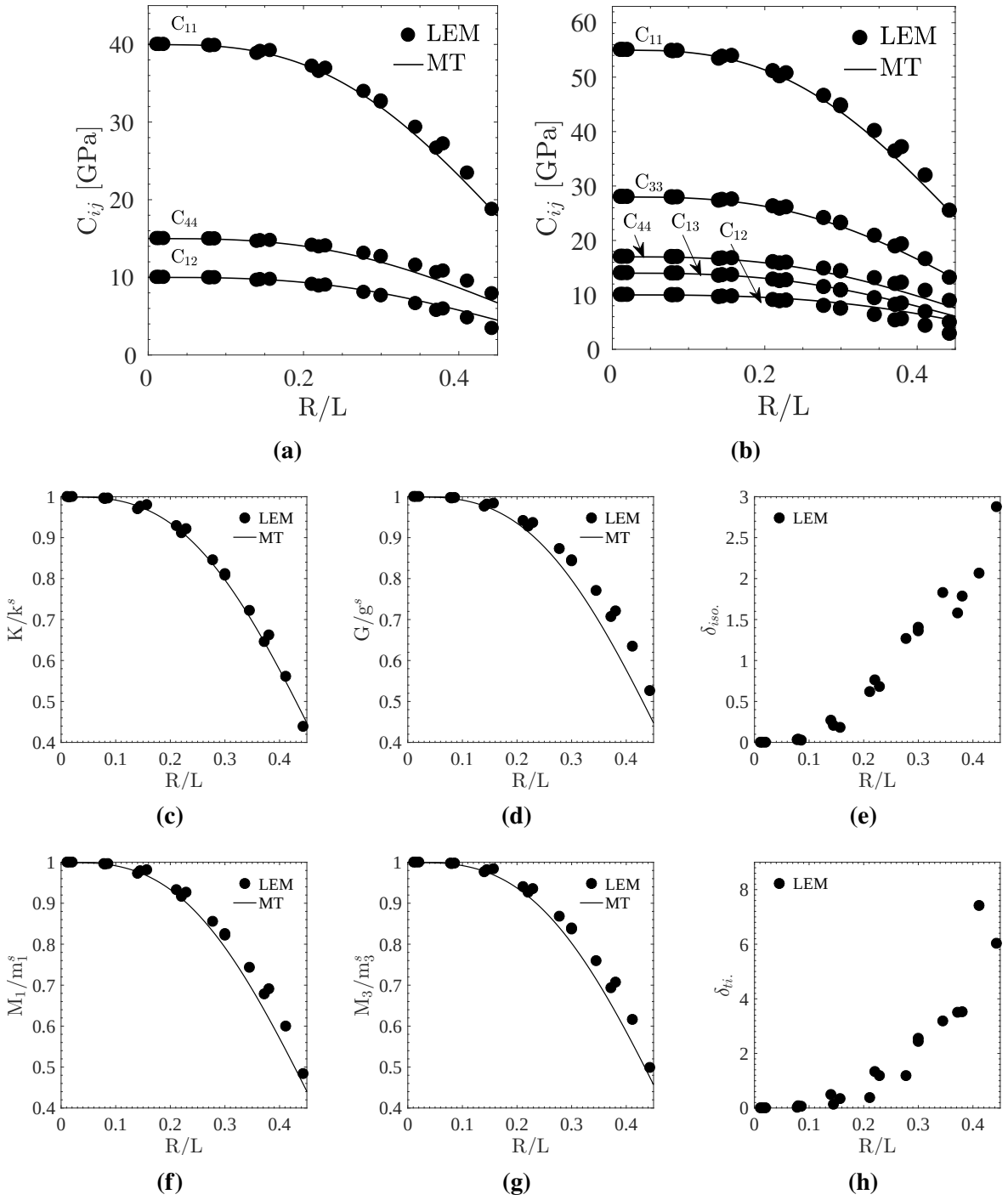
C11
C44
C12
LEM
MT
Cij [GPa]
R/L
(a)
C11
C33
C44
C13
C12
LEM
MT
Cij [GPa]
R/L
(b)
LEM
MT
K/k^s
R/L
(c)
LEM
MT
G/g^s
R/L
(d)
LEM
δiso.
R/L
(e)
LEM
MT
M1/m1^s
R/L
(f)
LEM
MT
M3/m3^s
R/L
(g)
LEM
δii.
R/L
(h)

Fig. 2

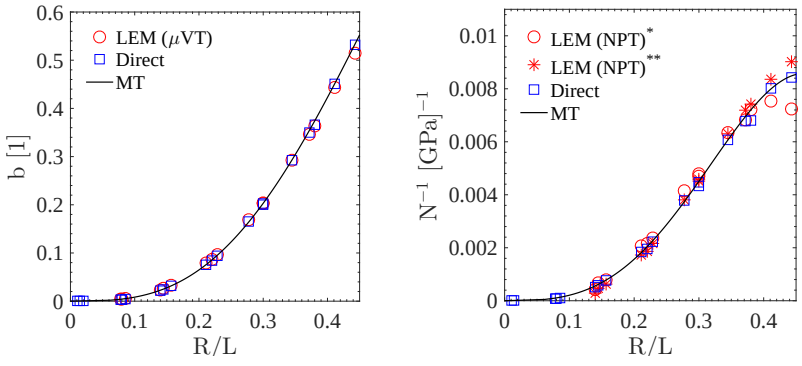

Fig. 3

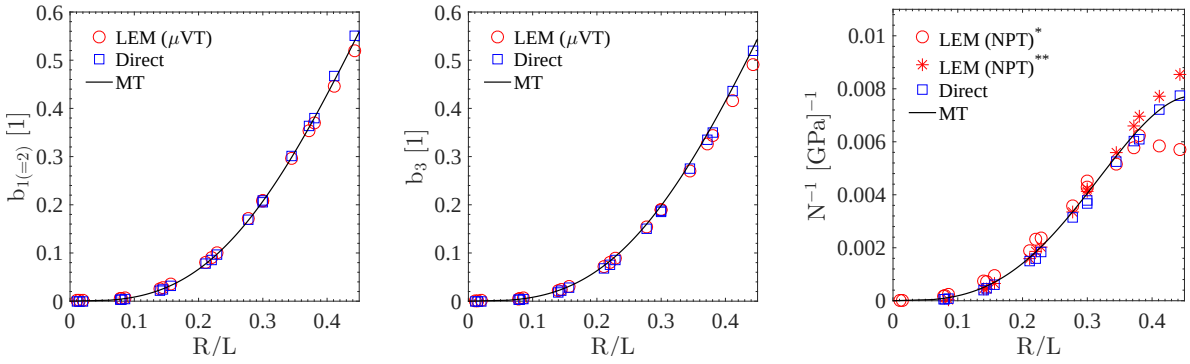
LEM (μVT)
Direct
MT
$b_{1(=2)}$ [1]
R/L
(a)
LEM (μVT)
Direct
MT
b_3 [1]
R/L
(b)
LEM (NPT)*
LEM (NPT)**
Direct
MT
N^{-1} [GPa]$^{-1}$
R/L
(c)

Fig. 4

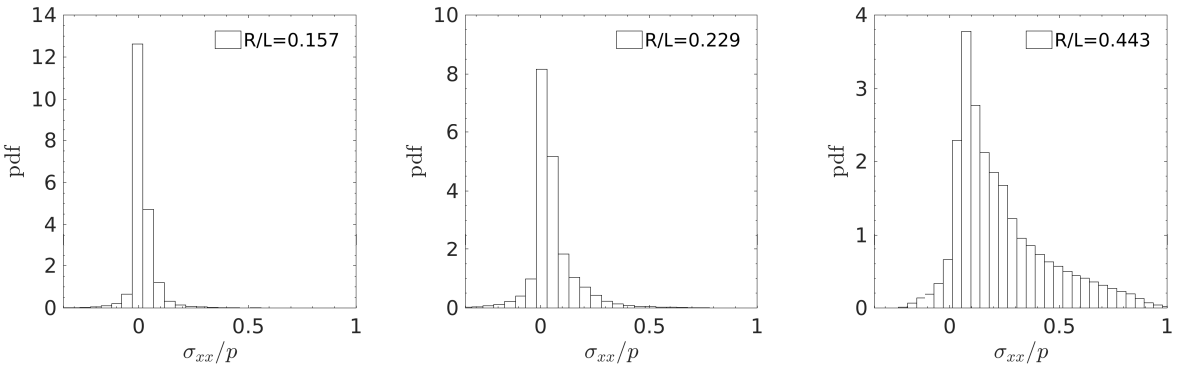
R/L=0.157
pdf
σ_{xx}/p
R/L=0.229
pdf
σ_{xx}/p
R/L=0.443
pdf
σ_{xx}/p

(a) **(b)** **(c)**

Fig. 5